Photoinduced tunability of the reststrahlen band in 4*H*-SiC

Bryan T. Spann,[1] Ryan Compton,[1] Daniel Ratchford,[1] James P. Long,[1] Adam D. Dunkelberger,[1] Paul B. Klein,[2] Alexander J. Giles,[1] Joshua D. Caldwell,[1,*] and Jeffrey C. Owrutsky[1,†]

[1] *U.S. Naval Research Laboratory, Washington, D.C. 20375, USA*

[2] *Sotera Defense Solutions Incorporated, Herndon, Virginia 20171, USA*

(Received 16 June 2015; revised manuscript received 22 January 2016; published 24 February 2016)

Materials with a negative dielectric permittivity (e.g., metals) display high reflectance and can be shaped into nanoscale optical resonators exhibiting extreme mode confinement, a central theme of nanophotonics. However, the ability to *actively tune* these effects remains elusive. By photoexciting free carriers in 4*H*-SiC, we induce dramatic changes in reflectance near the "reststrahlen band" where the permittivity is negative due to charge oscillations of the polar optical phonons in the midinfrared. We infer carrier-induced changes in the permittivity required for useful tunability ($\sim$40 cm^{-1}) in nanoscale resonators, providing a direct avenue towards the realization of actively tunable nanophotonic devices in the midinfrared to terahertz spectral range.

DOI: 10.1103/PhysRevB.93.085205

I. INTRODUCTION

The topic of subdiffractional light confinement has been at the forefront of modern photonics research for more than a decade, giving rise to the field of nanophotonics. Rapid advancements in this area have prompted considerable growth in the fields of nanoscale imaging, metamaterials, and chemical/biological sensing, among others. For example, the exploitation of surface plasmon polariton (SPP) resonances in metals has provided a means to achieve subdiffractional optical confinement, leading to strong localized fields and enhanced light-matter interactions from the ultraviolet (UV) to near infrared [1]. Alternatively, subdiffractional confinement of light can be produced at midinfrared to THz frequencies using polar dielectric materials such as SiC [2–6], hexagonal boron nitride (hBN) [7–9], and GaAs [10] via the excitation of surface phonon polaritons (SPhPs) [11]. Such polar dielectrics have attracted significant interest because their low optical losses yield comparatively high resonant quality factors [$Q = \omega_0/\Delta\omega$, where ω_0 and $\Delta\omega$ are the resonant frequency and corresponding full width at half maximum (FWHM)] for nanoparticle optical resonators. For example, theoretical Q's for a nanosphere exceed 900 in SiC compared to $\sim$40 for Ag, the typical metal of choice for low-loss plasmonics [12]. In addition, as we show here, the underlying dielectric permittivity of a polar semiconductor can be dynamically and significantly altered by introducing free carriers, thus providing the possibility for realizing active control of the optical and electronic properties of SPhP devices.

SPhPs arise from coherent charge oscillations supported by optical phonons of a polar lattice and can be stimulated when the real part of the material dielectric function becomes negative [3,4,12,13]. As with metals, this negative permittivity results in high reflectivity. For polar dielectrics, this occurs in the spectral region between the longitudinal- (LO) and transverse-optical (TO) phonon frequencies and is referred to as the "reststrahlen band", which depending on material, can be found in the spectral range from the midinfrared to THz ($\sim$6–350 μm). For example, in SiC the LO and TO phonon frequencies occur at about 970 cm^{-1}(10.3 μm) and 797 cm^{-1}(12.5 μm), resulting in high reflectivity in that range. Analogous to SPPs, SPhP fields are evanescent in character (confined to subdiffraction length scales near the surface) and can support both localized and propagating surface modes. Because the phenomenon is derived from optical phonons whose 1–10 ps scattering lifetimes are several orders of magnitude longer than free-carrier scattering, the optical losses are drastically lower for SPhPs, resulting in narrow resonance linewidths and high Q factors for subdiffractional polar dielectric nanostructures [2,3,5,6,8,12]. This has recently been demonstrated with experimental values extending upwards to $\sim$300 in SiC [5] and hBN [8] nanostructures.

One distinct advantage of SPhP modes is that the dielectric permittivity $\varepsilon(\omega)$ near and within the reststrahlen band, where $\text{Re}[\varepsilon(\omega)] \leqslant 0$, can be altered by introducing free carriers. This can be achieved either through electrostatic gating or optical pumping, thereby enabling the use of the LO-phonon free-carrier plasma coupling (LOPC) effect for *active tuning* of the SPhP modes in both traveling and localized resonator types [13–19]. The dielectric permittivity of polar dielectrics (e.g., 4*H*-SiC) can be expressed as a combination of a phononic term [in parentheses in Eq. (1)] and a Drude term [summation in Eq. (1)] [13]:

$$\varepsilon(\omega) = \varepsilon_\infty\left(1 + \frac{\omega_{\text{LO}}^2 - \omega_{\text{TO}}^2}{\omega_{\text{TO}}^2 - \omega^2 - i\omega\gamma}\right) - \sum_{j=e,h} \frac{N_j e^2}{\varepsilon_0 m_j^* m_0}\frac{1}{\omega^2 + i\omega\Gamma}, \quad (1)$$

where ε_∞ is the high-frequency permittivity, ω_{LO} is the LO phonon frequency, ω_{TO} is the TO phonon frequency, ω is the incident frequency, and γ is the damping constant. The free-carrier "Drude" contribution (subscripts e and h denote electrons and holes) is defined by the free-carrier density (N), the electron charge (e), the relative effective mass of the free carrier (m^*), electron mass (m_0), the vacuum permittivity (ε_0), and the plasmon damping constant (Γ) [12,20]. Since the background carrier concentration of $\sim 10^{14}$ cm^{-3} is much smaller than the concentration of the photoinjected carriers

*joshua.caldwell@nrl.navy.mil

†jeff.owrutsky@nrl.navy.mil

 ©2016 American Physical Society

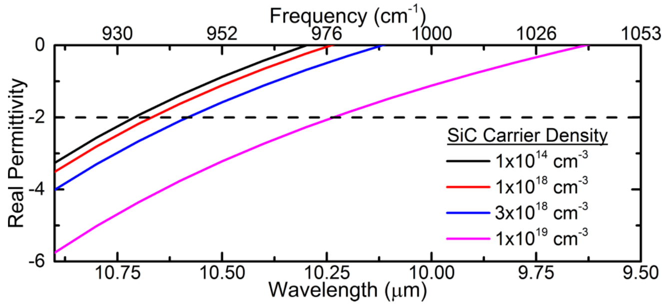

FIG. 1. The tunable nature of SiC permittivity as a function of wavelength for several values of photoinjected carrier density. The dashed line represents the spherical resonance condition in air.

generated in this work, we will consider $N_e = N_h \equiv N$ in the following. Controlling the permittivity can therefore be achieved by altering N via traditional doping, photoinjection, or electromodulation [14], as shown in Fig. 1, which plots the real part of the dielectric function for 4*H*-SiC in the presence of excess free carriers using typical 4*H*-SiC optical constants [13]. Within the electrostatic limit, the resonant frequency of a polaritonic nanoparticle (plasmon or phonon) occurs at a definite negative value of the permittivity depending on particle shape [20]. For a nanosphere in air, the resonant condition is $\mathrm{Re}[\varepsilon(\omega)] = -2$. Consulting Fig. 1, where this condition is plotted as a dashed line, one sees that for a spherical particle, its associated local SPhP resonance will blue-shift from approximately 10.75 μm (930 cm^{-1}) in the absence of free carriers to 10.3 μm (971 cm^{-1}) at carrier densities of approximately $1 \times 10^{19}\ \mathrm{cm}^{-3}$. Achieving such a shift with electro- or photomodulation of free carriers would represent a dynamic tunability, which cannot be reasonably achieved with SPPs in most plasmonic materials other than graphene [21,22], and could potentially facilitate a plethora of midinfrared to THz active nanophotonic applications.

Here we demonstrate the dynamic tunability of the permittivity for thick, epitaxially grown 4*H*-SiC in the vicinity of the reststrahlen band through the photoinjection of carriers. We use nanosecond pump-probe experiments to measure the free-carrier-induced reflection modulation arising from the LOPC effect. Large transient changes in reflectance are observed, increasing by nearly an order of magnitude at certain probe frequencies. This work differs in important ways from previous studies of the LOPC effect with ionized impurity doping [17]. First, in our work, the increased carrier density is transient in nature, which allows for fast-carrier modulation required for actively tunable SPhP devices. Second, photoinjected carriers may be subject to reduced scattering, specifically with respect to the losses induced by the presence of ionized dopant atom incorporation, prevalent with chemical doping. The results reported here exhibit rich spectral dynamics which provide an initial experimental demonstration of the phototunable nature of the permittivity in the vicinity of the reststrahlen band. By fitting our experimental results, we provide theoretical predictions on the anticipated magnitude of the spectral shift and induced losses under the active modulation of a spherical resonator. These experiments hence provide an initial step towards realizing actively tunable SPhP-based photonics.

II. RESULTS AND DISCUSSION

Measurements were carried out on a nominally undoped, 160 μm thick 4*H*-SiC epitaxial layer ($N \sim 10^{14}\ \mathrm{cm}^{-3}$) grown on a highly doped 4*H*-SiC substrate ($N \sim 3 \times 10^{18}\ \mathrm{cm}^{-3}$). The free carriers were injected into the epitaxial layer with a 355 nm pulsed laser, which has a penetration depth of approximately 50 μm [23], thereby ensuring all measured signals result only from the epilayer and are not coming from the underlying substrate. We employed a variable pump fluence F from 1 to $34\ \mathrm{mJ/cm}^2$, to provide a range of maximum absorbed photon densities $\Delta N_{\max}$ from $\sim 3 \times 10^{17}$ to $1 \times 10^{19}\ \mathrm{cm}^{-3}$ [$\Delta N_{\max} = \alpha(1-r)F/h\nu$, where h is Planck's constant and $\alpha = 210\ \mathrm{cm}^{-1}$, $r = 0.15$, and $\nu =$ 845 THz are the absorbance, reflectance, and pump frequency, respectively [23]]. The transient reflectance was probed with a continuous-wave, line-tunable CO_2 laser coupled with a fast mercury-cadmium-telluride detector that set the system temporal resolution to less than 100 ns. The pump and probe beams were both s polarized with angles of incidence of approximately 12° and 7° and beam diameters of 1.5 and 0.4 mm, respectively. The static reflectance spectrum was acquired with a Fourier-transform infrared spectroscopy (FTIR) spectrometer under identical angular and polarization conditions as the probe. The static and transient reflection spectra were fitted using Eq. (1) in WVASE ellipsometry software (J. A. Woolam, Inc.) to extract estimates of the free-carrier densities [24].

The static SiC reflection spectrum near the high-frequency (LO-phonon) side of the reststrahlen band is presented in Fig. 2 (black line) and demonstrates the high reflectivity that results from the screening field established by the polar optical phonons [12,20]. Changes in the SiC reflectance spectrum due to the injection of free carriers were probed at the available frequencies from the line-tunable CO_2 probe laser, denoted in Fig. 2 by the sets of dots that form coarse transient spectra. The red, green, and blue dots represent pump fluences of 1.0, 6.4, and $14.3\ \mathrm{mJ/cm}^2$, corresponding to instantaneous absorbed photon densities of $\Delta N_{\max} \sim 0.3 \times 10^{18}$, 2.0×10^{18}, and $4.6 \times 10^{18}\ \mathrm{cm}^{-3}$, respectively. We note that immediately after excitation, the free carriers will begin to recombine through Auger and surface recombination processes faster than our detector's temporal resolution. Therefore, the reflectance value at each fluence is actually the value induced by a free-carrier density somewhat lower than the maximum instantaneous value. The experimental data points presented in Fig. 2 were extracted from the transient-reflectance trace $\Delta R(t)/R_0$ [see Fig. 3 for representative $\Delta R(t)/R_0$ traces] for each probe frequency at time $t \sim 100$ ns (earliest time resolvable by our system) after the pump excitation and then multiplied by the baseline static reflectance. These data points were then scaled relative to the static-reflectance baseline.

The magnitudes of the transient reflectance signals exhibit a strong dependence on pump fluence, and the sign of the change depends upon the probe frequency. As demonstrated in Fig. 2, for increasing pump fluence, the reflectance decreases for probe frequencies within the reststrahlen band, while for frequencies along the band edge (~ 970–$990\ \mathrm{cm}^{-1}$) the reflectivity increases dramatically—by approximately an order of magnitude near $986\ \mathrm{cm}^{-1}$. This "softening" and shifting

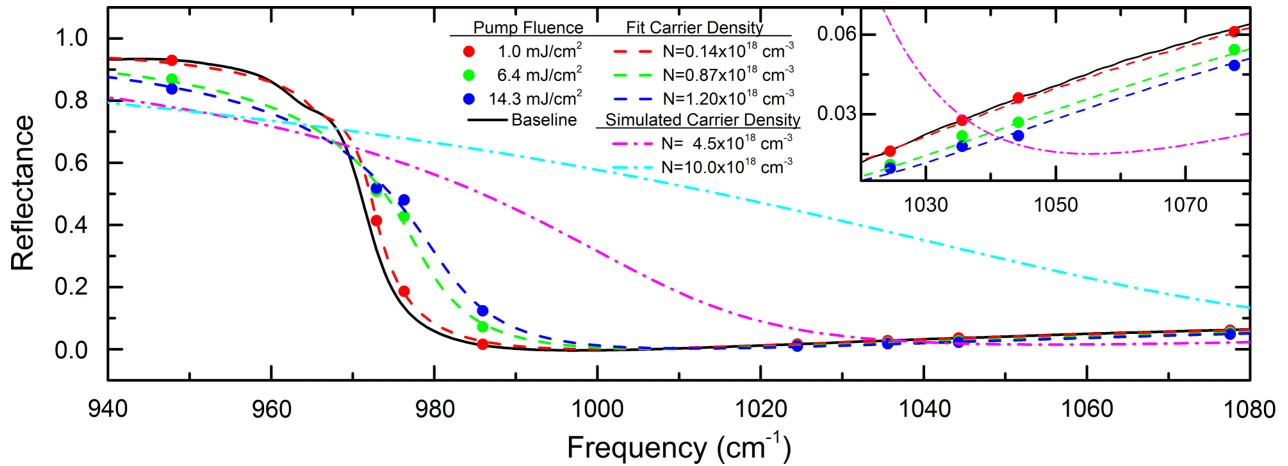

FIG. 2. Reflectance spectra of SiC following photoinjection (355 nm) at pump fluences of $F \sim 1.0\,\mathrm{mJ/cm^{-2}}$ (red dots), $6.4\,\mathrm{mJ/cm^{-2}}$ (green dots), and $14.3\,\mathrm{mJ/cm^{-2}}$ (blue dots) scaled relative to the baseline reflectance of the SiC sample (black line). Reflectance values were taken at the peak of the transient decay (~100 ns after excitation). The color-coordinated dashed lines are reflectance-spectra fits for the respective carrier densities (N). The dashed-dotted lines represent calculated reflectance curves for 4.5×10^{18} and $1 \times 10^{19}\,\mathrm{cm^{-3}}$ carrier densities. The inset shows the 1020−1080 cm^{-1} region rescaled.

of the reststrahlen band edge to higher frequencies (i.e., the reduced slope near the high-frequency edge) results from the coupling between the polar LO phonons and the free-carrier-induced plasma (i.e., the LOPC effect) [13,17].

Overlaid on the experimental measurements in Fig. 2 are calculated fits (dashed lines) to the set of transient-reflectance points (dots). For the fits, we employed the software WVASE, which computes reflectance with Fresnel equations incorporating the permittivity [Eq. (1)] in the appropriate tensor form for uniaxial 4H-SiC. A full list of the fitting values, as well as more details of the fitting procedure, are discussed in the Supplemental Material [24]. At $t \sim 100$ ns, the Drude term values determined from the fit were $N = 1.4 \times 10^{17}$, 8.7×10^{17}, and $1.2 \times 10^{18}\,\mathrm{cm^{-3}}$ and $\Gamma = 2.4 \times 10^{13}$,

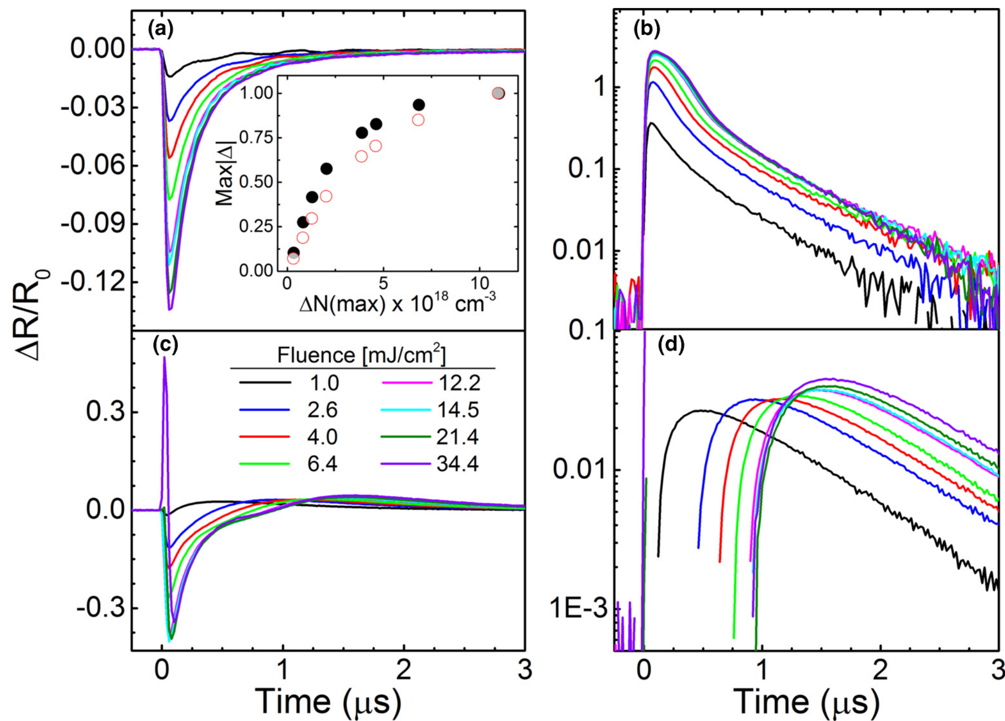

FIG. 3. Transient reflectance dynamics of SiC for various probe wavelengths [(a) 947.9 cm^{-1}, (b) 976.6 cm^{-1}, (c) 1043.8 cm^{-1}] near the blue edge of the reststrahlen band. The pump fluence was varied from $F \sim 1.0$ to $34.4\,\mathrm{mJ/cm^2}$, corresponding to photon densities of $\Delta N_{\max} \sim 0.33{-}11.0 \times 10^{18}\,\mathrm{cm^{-3}}$, for each probe wavelength. The inset of (a) shows the normalized peak change in reflectance at 947.9 cm^{-1} (solid black circles) and free-carrier absorption at 7692 cm^{-1} (open red circles) as a function of photoinjection density. (d) shows a semilogarithmic plot of the transient reflectance at 1043.8 cm^{-1} [from (c)].

7.7×10^{13}, and 8.0×10^{13} s^{-1} for the three fluences depicted by the red, green, and blue dashed lines in Fig. 2, respectively. The carrier densities evaluated from the actual absorption of the pump ($\Delta N_{max} = 3.0 \times 10^{17}$, 2.0×10^{18}, and 4.6×10^{18} cm^{-3}, plotted as the red, green, and blue dots of Fig. 2, respectively) are higher than the values obtained from the fitting procedure. This discrepancy is due to initial relaxation processes that occur within tens of nanoseconds that are not fully temporally resolved with our experimental setup [23,24].

Taking a closer look at the dynamics, Fig. 3, we observe markedly different transient-reflectance behaviors within, on the edge of, and to the high-frequency side of the reststrahlen band. Within the reststrahlen band [probe frequency of 947.9 cm^{-1}; Fig. 3(a)], the reflectance trace shows a monotonic decrease in reflectance as the pump power increases and all traces show a single exponential decay (∼700 ns) due to the subsequent recombination. We also determined the same ∼700 ns exponential decay from free-carrier absorption measurements probed at 7692 cm^{-1}(1.3 μm), far removed from the reststrahlen band, for every pump fluence (decays shown in the Supplemental Material). This exponential decay rate is consistent with measurements made previously on this sample by Ščajev *et al.* [23], who attribute it to Shockley-Read-Hall (SRH) recombination due to deep traps together with surface recombination [23]. Observation of the rapid nonlinear Auger decay expected for our higher injected carrier densities [23] is precluded by our detector's time resolution. However, the presence of this decay mechanism can be inferred from the fluence dependence of the normalized maximum change in reflectance at 947.9 cm^{-1} [solid black circles in the inset of Fig. 3(a)], which shows a linear trend for low ΔN_{max}, followed by a sublinear "roll-off" at higher pump densities. We find a very similar fluence dependence for the maximum change in transmittance in independent free-carrier absorption measurements performed at 7692 cm^{-1} [open red circles in the inset of Fig. 3(a)] [23]. The nonlinear behavior is a direct result of interband Auger recombination (for which the recombination rate scales as N^2) [23], an established recombination pathway in 4*H*-SiC for carrier densities in excess of $\sim 10^{18}$ cm^{-3}, similar to those used here [23]. Based on the strong similarity between the two sublinear sets of data in the inset of Fig. 3(a) measured at short time, and the correctly inferred exponential decay time of 700 ns at longer times, we conclude that carrier dynamics can be probed directly using changes in reflectance within the highly reflective region of the reststrahlen band. Further rationale is given in the Supplemental Material.

Unlike the transient decay rates measured within the reststrahlen band at 947.9 cm^{-1}, which are independent of carrier density, those measured on the steep high-frequency edge of the band at 976.6 cm^{-1} [Fig. 3(b)] exhibit a functional form that is nonexponential and carrier-density dependent at early times. In addition, as shown in Fig. 2, the reflectance here nearly tripled at the highest pump fluence. Similarly, at the ∼986 cm^{-1} probe (near the baseline reflectance minimum in the spectra in Fig. 2), the reflectance jumped nearly an order of magnitude at the highest pump fluence. Nagai *et al.* [25] observed similar dynamical changes in reflectance for GaN (>400%) using ultrafast techniques with finer time resolution. The complex decays and extreme reflectance changes are due to the high-frequency edge of the reststrahlen band sweeping to higher energy, a consequence of the hybridized LOPC mode mediated by the photoinjected carrier density N. This hybridized mode is comprised of upper (ω_+) and lower (ω_-) branches. As N is increased, ω_+ (near the LO-phonon frequency for low N) is driven to higher frequencies as it approaches the avoided crossing (defined by the plasma frequency), forcing significant changes in reflectance [26]. Harima *et al.* demonstrated this effect *statically* using Raman scattering of SiC epitaxial layers with different ionized dopant levels [13,17], while others have used modified graphene overlaid on SiC to *statically* tune the permittivity [27,28]. Our results indicate that the decay dynamics are nonexponential at longer times (after nonlinear Auger recombination becomes ineffective) because as the carriers recombine through the SRH and surface recombination mechanisms, the minimum in reflectance moves back from the blueshifted excited state, approaching the uncoupled LO-phonon position. This dynamic contribution from the carrier-dependent LOPC and various simultaneous recombination mechanisms provide for the complicated nonlinear response of the probe, making deconvolution of each phenomenon difficult. Nevertheless, the dynamic phototuning of reflectance caused by the carrier-modulated permittivity is clearly demonstrated.

More complicated transient behavior is observed in the higher-energy regions, past the reststrahlen band edge. In particular, at a probe frequency of 1043.8 cm^{-1} [Fig. 3(c)] at the highest photon density (i.e., $\Delta N_{max} > 1 \times 10^{19}$ cm^{-3}), $\Delta R(t)/R_0$ is initially positive, demonstrating a transient increase in reflectance. However, the sign of the transient reflectance rapidly becomes negative as the carrier density decreases. To account for this behavior, we calculated the reflectance spectra at the high carrier densities of 4.5×10^{18} and 1.0×10^{19} cm^{-3} (magenta and cyan dashed-dotted lines in Fig. 2, respectively). In the 1030–1040 cm^{-1} frequency range (see inset of Fig. 2), the calculations predict at the higher concentration that the reflectance should sharply increase, but as the carrier density decays below roughly 4×10^{18} cm^{-3} the reflectance should transition to a reflectance decrease, in qualitative agreement with our experiments. We note, however, that with further free-carrier recombination, our experiments exhibit $\Delta R(t)/R_0$ once again becoming positive for $\sim t > 200$ ns [Fig. 3(c)], a behavior not accounted for in our permittivity model. Eventually, the transient-reflectance decays exponentially back to the baseline with a time constant of ∼700 ns [see Fig. 3(d)] matching the free-carrier absorption dynamics discussed above.

Our analysis of the transient reflectance measurements provides insight into free-carrier-induced changes in the dielectric permittivity $\varepsilon(\omega)$. In our experiments, the positive spike feature in Fig. 3(c) is consistent with our calculations that free-carrier densities (N) of order 10^{19} cm^{-3} were photoinjected, even if they could not be directly probed temporally. Based on the modeled permittivity presented in Fig. 1 (real part of the permittivity), it is predicted that a spherical SiC resonator (dashed line in Fig. 1) would exhibit a spectral shift ($\delta\omega$) in excess of 40 cm^{-1} due to such a high free-carrier injection level. Such broad tuning of a resonance by rapid injection of carriers would be useful for a range of architectures, perhaps leading

to actively tunable midinfrared nanoscale optical antennas, waveguides, or epsilon-near-zero (ENZ) behavior [14].

While large spectral tuning is expected at high carrier densities, there is an important caveat to consider with regard to linewidth broadening of spectral resonances. As the carrier density increases and the Drude terms in Eq. (1) begin to dominate the dielectric function, one may expect broadening of the resonance due to the shorter scattering times of electrons compared to phonons. To determine the functionality of SPhP resonance tuning using carrier injection, we consider the simple model system of a spherical polar dielectric resonator with a radius a that is much smaller than the incident free-space wavelength (λ). The ratio of the sphere's absorption cross section to its geometric cross section is given by the following [20]:

$$Q_{\mathrm{abs}} = \frac{24\pi a}{\lambda} \frac{\varepsilon_m^{3/2}\varepsilon''}{(\varepsilon' + 2\varepsilon_m)^2 + \varepsilon''^2}. \quad (2)$$

Here, Q_{abs} is the absorption efficiency, not to be confused with the quality factor Q, with ε_m, ε', and ε'' representing the dielectric constant of the surrounding medium, and the real and imaginary parts of the complex dielectric function of the polar dielectric, respectively. In order to clearly illustrate our point, we make a simplifying approximation of an isotropic permittivity given by $\varepsilon = \varepsilon' + i\varepsilon''$. While 4*H*-SiC is technically a uniaxial crystal, previous studies have used this approximation to describe localized SPhP modes with excellent agreement [2,5,6]. Using the real and imaginary parts of the dielectric permittivity derived from Fig. 2 for each carrier density, we show the potential active tuning of a SiC spherical nanoresonator in air by plotting Q_{abs} in Fig. 4(a). As shown by Fig. 4, linewidth broadening accompanies the shifting of the peak because of the corresponding fast scattering rates of the photoinjected carriers. This is displayed more quantitatively in Fig. 4(b), which demonstrates that as the carrier density increases, the resonance exhibits a blue shift in the peak position along with increasing FWHM values. The additional broadening resembles results from previous Raman studies of doped SiC, which show apparent shifts and broadening of the LO-phonon band with increasing carrier concentration [17,18]. Based on the estimated permittivities derived from Fig. 2, we would expect a spectral shift $\delta\omega$ of about 5 cm^{-1} at a injected carrier density of $1.2 \times 10^{18}\ \mathrm{cm}^{-3}$ with the resonance linewidth, $\Delta\omega = 8\ \mathrm{cm}^{-1}$, corresponding to a modulation depth of $\delta\omega/\Delta\omega = 0.6$ and a quality factor of $\omega/\Delta\omega = 120$. Therefore, even given the additional broadening, the quality factor is still significantly higher than any reported plasmonic systems (a survey of such Q factors in both SPP and SPhP materials may be found in Ref. [11]), and the modulation depth is comparable to the highest tuning ranges reported for plasmonic systems [29,30]. Additionally, a major benefit of the tuned SPhPs is that their linewidths are much narrower than their plasmonic counterparts, so the former could potentially be applied to modulated surface-enhanced IR (SEIRA) techniques.

As mentioned above, the temporally unresolved positive feature in Fig. 3(c) suggests we are approaching carrier densities of $\sim 10^{19}\ \mathrm{cm}^{-3}$. Figure 4(a) includes calculated curves for carrier densities of 4.5×10^{18} and $1.0 \times 10^{19}\ \mathrm{cm}^{-3}$ (dashed lines) to show the potential tunability of the resonances at higher carrier densities. For these two higher carrier densities,

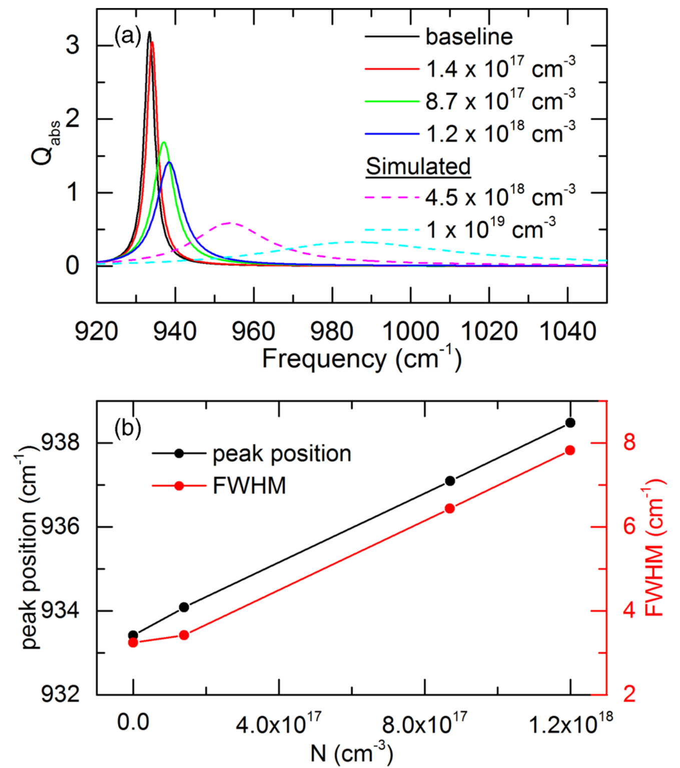

FIG. 4. Theoretical spherical surface phonon polariton resonance tuning of a 50-nm-radius SiC nanoresonator. Solid lines in (a) are calculated from the permittivity values derived from Fig. 2. The lines are labeled based on the estimated carrier density. The dashed lines in (a) represent simulated tuning for carrier densities of 4.5×10^{18} and $1 \times 10^{19}\ \mathrm{cm}^{-3}$. (b) plots the resonant peak positions and FWHM values of the experimental data from this study [solid lines in (a)].

we let the free-carrier-induced damping be fixed at the maximum value derived from our fits, i.e., $\Gamma = 8.0 \times 10^{13}\ \mathrm{s}^{-1}$. At the highest carrier density of $1 \times 10^{19}\ \mathrm{cm}^{-3}$, the resonance shifts by $>40\ \mathrm{cm}^{-1}$. Note, however, that even though the Drude damping parameter was kept constant for the carrier densities of 1.2×10^{18}, 4.5×10^{18}, and $1 \times 10^{19}\ \mathrm{cm}^{-3}$ (which correspond to plasma frequencies of 506, 980, and 1461 cm^{-1}), the resonance linewidth still shows significant broadening for the highest carrier densities. This large increase in linewidth is relatively insensitive to the value of the damping parameter. For example, doubling the Drude damping parameter from 8.0×10^{13} to $16 \times 10^{13}\ \mathrm{s}^{-1}$ only increases the linewidth from approximately 55 to 70 cm^{-1}. This large increase in resonance linewidth at higher carrier densities occurs because the Drude term begins to dominate the SiC dielectric function as the plasma frequency approaches ω_{LO}. At a carrier density of $1 \times 10^{19}\ \mathrm{cm}^{-3}$ ($4.5 \times 10^{18}\ \mathrm{cm}^{-3}$), we calculate a modulation depth of about 1 (0.9) and a quality factor of roughly 18 (42). Therefore, even with significant broadening due to increased carrier-carrier scattering from the photoinjection, there is potential to actively tune nanoresonators over large spectral regions while maintaining comparable figures of merit to traditional plasmonic systems.

While we have demonstrated the carrier-induced transient tuning of the dielectric function of 4*H*-SiC through optical pumping, this effect can also be potentially realized through

carrier injection within electronic devices; for instance, gated transistor architectures or bipolar electronic devices (e.g., *p-i-n* diodes). When coupled with the controllable carrier recombination times ranging from the picoseconds to tens of microseconds [31] in direct- and indirect-band-gap semiconductors, respectively, the active tunability provided by carrier injection demonstrated here presents a clear path towards modulated and active photonic devices in the midinfrared to THz spectral ranges.

III. CONCLUDING REMARKS

In conclusion, we have employed transient infrared pump-probe spectroscopy with variable levels of photocarrier injection to explore the effects of free carriers in the reststrahlen band region of SiC. The pump-probe experiments revealed complex transient behavior that provides evidence for the LOPC-mediated carrier-tunable permittivity of 4*H*-SiC. By fitting the transient reflectance spectra with a model of permittivity that included phononic and free-carrier terms, we are able to extract estimates of the free-carrier densities and carrier-induced damping under various optical pumping levels. The inferred carrier-induced changes in the dielectric permittivity enable the prediction of the potential for active tunability of SPhP architectures. For example, at our highest pump fluence ($34\,\mathrm{mJ/cm^2}$) the reflectance behavior implies a carrier density of $\sim 10^{19}\,\mathrm{cm^{-3}}$, which predicts a $\sim 40\,\mathrm{cm^{-1}}$ shift for the local SPhP resonance in a SiC nanosphere. This suggests prospective photomodulation in these polar dielectrics over an order of magnitude greater than the modulation depth of other active nanophotonic approaches. Hence, the results provided here indicate the potential for achieving dynamic tunability of localized SPhP modes in subdiffractional optical antennas [2,5,6,8], waveguides [12,14], and ENZ-based effects. Such functionality would provide a novel approach towards realizing active nanophotonics in the midinfrared to THz frequency regions at modulation frequencies from the kHz to GHz.

ACKNOWLEDGMENTS

The authors wish to acknowledge support from the U.S. Office of Naval Research through the Naval Research Laboratory Nanoscience Institute. B.T.S, R.C., A.D.D., and A.J.G. thank the National Research Council for support in administering their postdoctoral fellowships at NRL. The authors would like to thank Igor Vurgaftman (NRL), Chris Kendziora (NRL), Orest Glembocki (NRL), and Jon Schuller (University of California–Santa Barbara) for helpful discussions.

B.T.S. and R.C. contributed equally to this work.

[1] S. A. Maier, *Plasmonics: Fundamentals and Applications* (Springer, New York, 2007).
[2] J. D. Caldwell *et al.*, Nano Lett. **13**, 3690 (2013).
[3] R. Hillenbrand, T. Taubner, and F. Keilmann, Nature (London) **418**, 159 (2002).
[4] J.-J. Greffet, R. Carminati, K. Joulain, J.-P. Mulet, S. Mainguy, and Y. Chen, Nature (London) **416**, 61 (2002).
[5] Y. Chen *et al.*, ACS Photonics **1**, 718 (2014).
[6] T. Wang, P. Li, B. Hauer, D. N. Chigrin, and T. Taubner, Nano Lett. **13**, 5051 (2013).
[7] S. Dai *et al.*, Science **343**, 1125 (2014).
[8] J. D. Caldwell *et al.*, Nat. Commun. **5**, 5221 (2014).
[9] X. G. Xu, B. G. Ghamsari, J.-H. Jiang, L. Giburd, G. O. Andreev, C. Zhi, Y. Bando, D. Goldberg, P. Berini, and G. C. Walker, Nat. Commun. **5**, 4782 (2014).
[10] S. A. Holmstrom, T. H. Stievater, M. W. Pruessner, D. Park, W. S. Rabinovich, J. B. Khurgin, C. J. K. Richardson, S. Kanakaraju, L. C. Calhoun, and R. Ghodssi, Phys. Rev. B **86**, 165120 (2012).
[11] J. D. Caldwell, L. Lindsey, V. Giannini, I. Vurgaftman, T. Reinecke, S. A. Maier, and O. J. Glembocki, Nanophotonics **4**, 44 (2015).
[12] J. D. Caldwell, L. Lindsay, V. Giannini, I. Vurgaftman, T. L. Reinecke, S. A. Maier, and O. J. Glembocki, Nanophotonics **3**, 2192 (2014).
[13] T. E. Tiwald, J. A. Woollam, S. Zollner, J. Christiansen, R. B. Gregory, T. Wetteroth, S. R. Wilson, and A. R. Powell, Phys. Rev. B **60**, 11464 (1999).
[14] J. P. Long, J. D. Caldwell, J. C. Owrutsky, and O. J. Glembocki, U.S. Patent No. 9,195,052 B2 (24 November 2015).
[15] M. Chafai, A. Jaouhari, A. Torres, R. Antón, E. Martın, J. Jimenez, and W. Mitchel, J. Appl. Phys. **90**, 5211 (2001).
[16] H. Altan, X. Xin, D. Matten, and R. Alfano, Appl. Phys. Lett. **89**, 052110 (2006).
[17] H. Harima, S.-i. Nakashima, and T. Uemura, J. Appl. Phys. **78**, 1996 (1995).
[18] J. D. Caldwell, O. J. Glembocki, S. M. Prokes, E. R. Glaser, K. D. Hobart, D. M. Hansen, G. Chung, A. V. Bolotnikov, and T. S. Sudarshan, J. Appl. Phys. **101**, 093506 (2007).
[19] A. Mooradian and G. Wright, Phys. Rev. Lett. **16**, 999 (1966).
[20] C. F. Bohren and D. R. Huffman, *Absorption and Scattering of Light by Small Particles* (Wiley, New York, 2008), p.331.
[21] Z. Fei *et al.*, Nature (London) **487**, 82 (2012).
[22] J. Chen *et al.*, Nature (London) **487**, 77 (2012).
[23] P. Ščajev, V. Gudelis, K. Jarašiūnas, and P. B. Klein, J. Appl. Phys. **108**, 023705 (2010).
[24] See Supplemental Material at http://link.aps.org/supplemental/10.1103/PhysRevB.93.085205 for additional information on experimental details, calculations and corresponding assumptions, and free-carrier absorption data.
[25] M. Nagai, K. Ohkawa, and M. Kuwata-Gonokami, Appl. Phys. Lett. **81**, 484 (2002).
[26] J. Steele *et al.*, Opt. Express **22**, 11680 (2014).
[27] B. K. Daas, K. M. Daniels, T. S. Sudarshan, and M. V. S. Chandrashekhar, J. Appl. Phys. **110**, 113114 (2011).
[28] B. K. Daas and A. Dutta, J. Mater. Res. **29**, 2485 (2014).
[29] A.-K. U. Michel, D. N. Chigrin, T. W. Maß, K. Schönauer, M. Salinga, M. Wuttig, and T. Taubner, Nano Lett. **13**, 3470 (2013).
[30] Z. Samson, K. MacDonald, F. De Angelis, B. Gholipour, K. Knight, C. Huang, E. Di Fabrizio, D. Hewak, and N. Zheludev, Appl. Phys. Lett. **96**, 143105 (2010).
[31] S. Ichikawa, K. Kawahara, J. Suda, and T. Kimoto, Appl. Phys. Express **5**, 101301 (2012).